JGR Solid Earth

RESEARCH ARTICLE
10.1029/2020JB020237

Special Section:
Ophiolites and Oceanic Lithosphere, with a focus on the Samail ophiolite in Oman

A Mg Isotopic Perspective on the Mobility of Magnesium During Serpentinization and Carbonation of the Oman Ophiolite

Juan Carlos de Obeso[1,2], Danielle P. Santiago Ramos[3,4], John A. Higgins[3], and Peter B. Kelemen[1,5]

[1]Lamont Doherty Earth Observatory, Columbia University, Palisades, NY, USA, [2]Now at Department of Geoscience, University of Calgary, Calgary, AB, Canada, [3]Department of Geosciences, Princeton University, Princeton, NJ, USA, [4]Now at Geology and Geophysics, Woods Hole Oceanographic Institution, Woods Hole, MA, USA, [5]Department of Earth and Environmental Sciences, Columbia University, Palisades, NY, USA

Abstract Alteration of mantle peridotite in the Samail ophiolite forms secondary minerals, mainly serpentine and Mg-rich carbonates. Magnesium accounts for ~25 – 30% of peridotite mass and its mobility can be used to trace this alteration. We report the first set of Mg isotope measurements from peridotites and their alteration products in Oman. Partially serpentinized peridotites have Mg isotope ratios that are indistinguishable from estimates for the average mantle and bulk silicate earth (δ^{26}Mg = −0.25 ± 0.04‰). However, more extensively altered peridotite samples show large shifts in Mg isotopic composition. The range of δ^{26}Mg values for our suite of alteration products from the mantle section is ~4.5‰ (from −3.39‰ to 1.19‰), or >60% of the total range of terrestrial variability in δ^{26}Mg values. Serpentine veins are typically enriched in ^{26}Mg (max δ^{26}Mg value = 0.96‰) whereas Mg-carbonate veins are associated with low ^{26}Mg/^{24}Mg ratios (magnesite δ^{26}Mg = −3.3‰, dolomite δ^{26}Mg = −1.91‰). Our preferred explanation for the range in δ^{26}Mg values involves coprecipitation of serpentine and carbonates at water-to-rock ratios >10^3. The coincidence of alteration products characterized by δ^{26}Mg values that are both lower and higher than bulk silicate Earth and the finite ^{14}C ages of the carbonates suggest that both serpentinization and carbonation are ongoing in Oman. Rates of calcite precipitation in travertines inferred from $\Delta^{26}Mg_{cal\text{-}fl}$ suggest that travertine formation in Oman sequesters a total of 10^6–10^7 kg CO_2/yr, consistent with previous estimates.

Key Points:

- The range of δ^{26}Mg from samples of the mantle section in the Oman ophiolite is ~4.5‰, or >60% of the total range of terrestrial variability
- The range in δ^{26}Mg values involves coprecipitation of serpentine and carbonates at high water-to-rock ratios
- Serpentinization and carbonation are ongoing in the mantle section of the Oman ophiolite

Supporting Information:

- Supporting Information S1

Correspondence to:
J. C. de Obeso,
juancarlos.deobeso@ucalgary.ca

Citation:
de Obeso, J. C., Santiago Ramos, D. P., Higgins, J. A., & Kelemen, P. B. (2021). A Mg isotopic perspective on the mobility of magnesium during serpentinization and carbonation of the Oman ophiolite. *Journal of Geophysical Research: Solid Earth*, *126*, e2020JB020237. https://doi.org/10.1029/2020JB020237

Received 21 MAY 2020
Accepted 2 DEC 2020

1. Introduction

Alteration of ultramafic rocks is ubiquitous in near-surface environments, both on land and below the seafloor. Mantle olivine and pyroxene are unstable at near-surface conditions and undergo hydration (serpentinization) and carbonation when fluids are present (e.g., Moody, 1976). These reactions result in the formation of serpentine minerals, carbonates, brucite, magnetite, and other Fe-oxides and hydroxides. Serpentinization and carbonation reactions are often nearly isochemical apart from the addition of H_2O and CO_2 (e.g., Coleman & Keith, 1971). Both observations and thermodynamic modeling suggest that changes in major element ratios such as Si/Mg are minor (e.g., ≤10% for low-temperature reaction with seawater, Figure 3 in Malvoisin, 2015; Monnier et al., 2006; Snow & Dick, 1995). However, other studies (e.g., Al-Khirbash, 2015; Auclair et al., 1993; Beinlich et al., 2018; de Obeso & Kelemen, 2018, 2020; Esteban Guzman et al., 2011; Hotz, 1964; Nasir et al., 2007; Skarpelis, 2006) have shown that under certain conditions mass transfer during serpentinization can lead to larger changes in major element chemistry. In Oman, partially serpentinized harzburgites record a ~2% decrease in Mg compared to the inferred composition of unaltered mantle peridotites (Monnier et al., 2006), with examples of heavily altered harzburgite that have lost up to 30% of their original Mg (de Obeso & Kelemen, 2020).

Magnesium isotope studies show that the composition of the mantle and bulk silicate earth (BSE) is relatively uniform, with δ^{26}Mg values = −0.25 ± 0.04‰ (2σ) (Teng, 2017; Teng et al., 2010). Liu et al. (2017) report δ^{26}Mg values of −0.12 ± 0.13‰ (2σ) for altered seafloor peridotites. There are a limited number of studies on magnesium isotope compositions of ophiolite peridotites. Peridotites from the Purang ophiolite (Tibet) have δ^{26}Mg = −0.20 ± 0.10‰ (2σ), within uncertainty of mantle compositions (Su et al., 2015) and

peridotites from the Feragen and Linnajavri ultramafic bodies (Norway) have mantle-like Mg isotope ratios, with δ^{26}Mg values ranging from −0.35‰ to −0.23‰ (Beinlich et al., 2014).

Magnesium isotopes are known to fractionate during precipitation of carbonates and silicates from aqueous fluids. This fractionation can be used to constrain alteration processes during serpentinization and carbonation. Carbonates preferentially incorporate ^{24}Mg during crystallization, as observed in both experimental and natural samples, which yield large fractionation factors (Higgins & Schrag, 2010; Li et al., 2015; Mavromatis et al., 2013; Pearce et al., 2012; Shirokova et al., 2013; Tipper et al., 2006). On the other hand, available constraints on Mg fractionation factors associated with formation of serpentine polymorphs are equivocal. For example, based on dissolution experiments of San Carlos olivine at low temperature (~25°C), Wimpenny et al. (2010) suggested that chrysotile preferentially removed light Mg from solution. In contrast, Ryu et al. (2016) synthetized lizardite from solution and reported that the mineral product was enriched in heavy Mg relative to the fluid at experimental temperatures of 90 and 250°C. Following a molecular dynamics approach, Wang et al. (2019) also concluded that lizardite crystallization preferentially removes ^{26}Mg from the fluid. These experimental results contrast with fractionation estimates based on natural samples that concluded that serpentinization does not fractionate Mg isotopes (Beinlich et al., 2014; Liu et al., 2017; Oskierski et al., 2019). Studies of natural samples also suggest that talc and Mg-rich clays formed during alteration are enriched in ^{26}Mg (Beinlich et al., 2014; Liu et al., 2017) in contrast with recent experimental studies that showed preferential incorporation of ^{24}Mg in stevensite and saponite (Hindshaw et al., 2020). In summary, whereas carbonate/water fractionation factors are large, those for serpentine are uncertain but close to 1. Thus, Mg isotopes should be sensitive to the conditions of serpentinization and carbonation.

To explore the behavior of Mg and Mg isotopes during serpentinization and carbonation, we present the first suite of Mg isotope analyses of bulk-rock samples and mineral separates from the Samail ophiolite in Oman. Our sample suite consists of 37 samples of harzburgites and dunites with different degrees of alteration, as well as products of peridotite alteration (silicates and carbonates). We find that although the Mg isotopic compositions of partially serpentinized Oman peridotites (average δ^{26}Mg = −0.25 ± 0.14‰, 2σ) are indistinguishable from mantle values, serpentine and carbonate samples are ^{26}Mg-enriched (max. δ^{26}Mg value = 0.96‰) and ^{26}Mg-depleted (min. δ^{26}Mg value = −3.38‰), respectively, compared to average mantle. We explore different hypotheses to explain the co-occurrence of high δ^{26}Mg serpentines and low δ^{26}Mg carbonates and discuss results in the context of previously published ^{14}C analyses which indicate that serpentinization and carbonation are ongoing during weathering of the Samail ophiolite mantle section.

2. Geological Background and Sample Selection

The Samail ophiolite in eastern Oman is the best-exposed section of oceanic crust and mantle in the world (Figure 1). The mantle section of the ophiolite is composed of highly depleted harzburgites together with ~5%–15% dunite (Boudier & Coleman, 1981; Braun, 2004; Braun & Kelemen, 2002; Collier, 2012). These peridotites exhibit different degrees of alteration ranging from ~30% serpentinized in "fresh" rocks to instances of completely serpentinized (Godard et al., 2000; Monnier et al., 2006) and completely carbonated peridotites (Falk & Kelemen, 2015; Nasir et al., 2007; Stanger, 1985). There is substantial evidence that alteration occurred throughout the history of the ophiolite. δ^{18}O data suggest that some alteration occurred near the axis of the spreading center as seawater interacted with the Samail crust (Gregory & Taylor, 1981), an internal ^{87}Sr/^{86}Sr isochron on listvenite (carbonated peridotite) shows that alteration continued during obduction and emplacement (Falk & Kelemen, 2015). The presence of hyperalkaline springs, recently crystallized carbonate veins and highly reduced fluids and mineral assemblages indicates that alteration is ongoing (e.g., Chavagnac et al., 2013a, 2013b; Clark & Fontes, 1990; Coleman & Keith, 1971; Kelemen et al., 2011; Kelemen & Matter, 2008; Mervine et al., 2014; Monnin et al., 2011; Neal & Stanger, 1985; Streit et al., 2012).

Previous studies of low-temperature alteration of the Oman ophiolite propose that it occurs in three steps (e.g., Barnes et al., 1978, 1967; Barnes & O'Neil, 1969; Chavagnac et al., 2013a; Kelemen et al., 2011; Neal & Stanger, 1985; Noël et al., 2018; Paukert et al., 2012). Step 1 is characterized by formation of Mg^{2+}-HCO_3^- rich fluids, as atmospheric CO_2 bearing rainwater dissolves Mg from peridotite during near-surface weathering. These fluids have exchange with the atmosphere and inferred to be 0–40 years old (Paukert Vankeuren et al., 2019). During step 2, this so-called "Type I" water percolates deeper into peridotite leading to

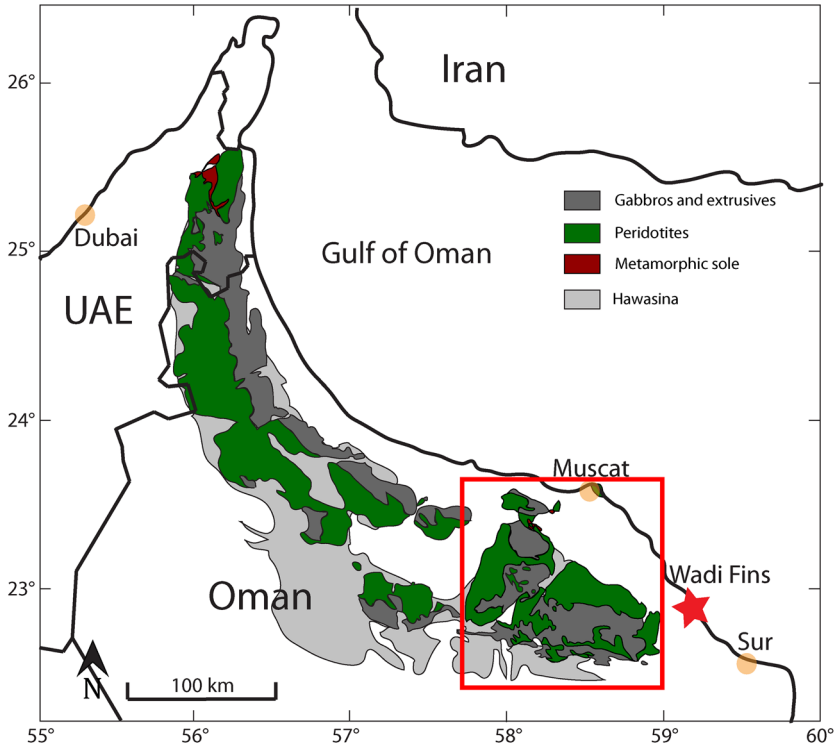

Figure 1. Simplified geologic map of the Samail ophiolite in Oman and the United Arab Emirates. All samples in this study come from the southern massifs (red square) and a small exposure beneath overlying Cretaceous to Eocene limestones at Wadi Fins (red star). Modified after Nicolas et al. (2009).

precipitation of Mg-rich carbonates, brucite, and serpentine. These reactions remove carbon and Mg^{2+} from the fluid and dissolve Ca^{2+}, which is incompatible in the alteration minerals. The resulting fluids, known as "Type II" waters, have low Mg and C, high Ca and pH, and very low oxygen fugacities (Bruni et al., 2002; Clark & Fontes, 1990; Neal & Stanger, 1983; Paukert et al., 2012). During step 3, hyperalkaline "Type II" fluids are returned to the surface, where disequilibrium with the atmosphere leads to rapid uptake of atmospheric CO_2 and precipitation of calcite to form travertine deposits (Chavagnac et al., 2013a; Clark & Fontes, 1990; Kelemen & Matter, 2008; Kelemen et al., 2011; Mervine et al., 2014; Neal & Stanger, 1985; Paukert et al., 2012).

Magnesium fluxes during these three stages of alteration remain poorly constrained but inferences of water/rock during alteration have been made for Oman peridotites. Observations in partially serpentinized peridotites of sulfide, and in some cases native metals recording low oxygen fugacities, are associated with low water/rock ratios (W/R) and incipient serpentinization (de Obeso & Kelemen, 2020; Frost, 1985; Kelemen et al., 2020; Lorand, 1988). Increased W/R are inferred from changes in accessory sulfide minerals (de Obeso & Kelemen, 2020) and the occurrence of diffuse carbonate vein networks in the peridotites (Noël et al., 2018). Even higher W/R are expected to have been involved in the formation of massive carbonate-serpentine veins which acted as main fluid paths for fluids interacting with peridotites (de Obeso & Kelemen, 2018; Noël et al., 2018). Secondary minerals from the three steps formed at variable W/R have different aqueous Mg^{2+}-mineral fractionation properties with silicates expected to become enriched in ^{26}Mg and carbonates enriched in ^{24}Mg (e.g., Beinlich et al., 2014; Gao et al., 2018; Liu et al., 2017; Pinilla et al., 2015; Wang et al., 2019; Wimpenny et al., 2014) suggesting that Mg isotopes can be used as tracers of alteration.

All samples analyzed here were collected from the southern massifs of the ophiolite, within its mantle section (Figure 1). Timing of alteration/crystallization of most samples is unknown and samples might reflect multiple alteration episodes over the 95 million years since the ophiolite was emplaced. We assume that even if some samples record old serpentinization and carbonation reactions they are appropriate recorders of ongoing processes. Previously described samples analyzed for this study can be separated into

silicate-bearing and carbonate-bearing groups. Silicate samples include relatively fresh harzburgites ($n = 6$, average ~40% relict mantle minerals) and dunites ($n = 4$, ~23%) from Hanghøj et al. (2010), highly serpentinized harzburgites ($n = 2$, 37% and 14%) and dunites ($n = 1$, 0%) from de Obeso and Kelemen (2018), and a set of serpentinized harzburgites ($n = 3$, ~40%), high-Si harzburgite ($n = 3$, 0%), and oxidized harzburgite ($n = 3$, 0%) from de Obeso & Kelemen, 2020. We also include four samples not previously described: two serpentine veins, one serpentinite, and a material from a vein within a serpentinized body with Mg/Si~1 and waxy texture that we refer to as a "waxy vein."

Carbonate samples include two groups: completely carbonated peridotites, also known as listvenites, from Falk and Kelemen (2015), further classified as dolomite listvenites ($n = 2$) and magnesite listvenites ($n = 2$). We also analyzed massive carbonate veins from serpentinized peridotite outcrops, including two magnesite veins and one dolomite vein (Kelemen et al., 2011). The three carbonate vein samples have ^{14}C contents corresponding to ages of 32, 37, and 40 ka (Kelemen et al., 2011). Two travertine samples from Kelemen et al. (2011) were also analyzed. These travertines are composed mainly of calcite (XRD calcite contents 88.3% and 91.4%), with ^{14}C contents corresponding to ages of 1,630 and 18,450 years. We also include two carbonate vein samples not previously described: a massive magnesite vein and a huntite ($CaMg_3(CO_3)_4$) vein. Major element compositions and locations for the new samples are reported in Table S1.

3. Methods

Samples not previously described (four silicates and two carbonates) were processed in Lamont Doherty Earth Observatory (LDEO). Samples were chipped using a jaw crusher and powdered using an alumina puck mill. Major element analyses and loss on ignition (LOI) were performed at LDEO. Major elements were measured on an Agilent 720 Axial ICP-OES calibrated with rock standards (Table S2) following dissolution by lithium metaborate fusion and nitric acid.

For Mg isotopic analyses powders of all 37 samples and three USGS rock standards (BCR-2, BHVO-2, BIR-1A) were digested using a HNO_3:HF (3:1) digestion procedure at LDEO. Sample OM17-magnesite was processed in multiple digestion batches to check reproducibility ($n = 5$). Once digested, <1 μg of Mg from each sample was purified from the silicate/carbonate matrix using a Thermo Dionex 5000+ ion chromatography (IC) system at Princeton University. The procedure for both carbonate and silicate minerals is described in more detail in Husson et al. (2015) and Santiago Ramos et al. (2020).

Isotopic analyses were carried out at Princeton University on a Thermo Fisher Scientific Neptune Plus MC-ICP-MS from purified solutions with Mg concentrations of 150 ppb in low mass resolution using a quartz spray chamber. There are no major isobaric interferences in the masses of interest. Standard-sample-standard bracketing was used to correct for instrumental mass fractionation (Galy et al., 2001) and values were normalized to an internal standard (DSM-3). Magnesium isotope ratios are reported using delta notation. Long-term external reproducibility is estimated by comparing Mg standard Cambridge-1 against DSM-3 standard. Measured δ^{26}Mg values for Cambridge-1 yield an average of -2.59 ± 0.05‰ (2σ, $n = 7$), indistinguishable from the published value of -2.62 ± 0.03‰ (2σ) (Galy et al., 2003; Teng et al., 2015). Reported uncertainties for each sample depend on the number of times the sample has been separated and analyzed. For a single separation and analysis, we report the long-term external reproducibility of Cambridge-1 (δ^{26}Mg $2\sigma = \pm 0.09$‰). For multiple chromatographic separations and analyses ($n > 1$), we report each duplicate. USGS standards ran as unknowns are reported in Table S3. All analyzed samples fall on an isotopic mass-dependent fractionation line in three-isotope space with slope of 0.5196 ± 0.0024 ($R^2 = 0.9992$), indistinguishable from the value of 0.5210 estimated for equilibrium fractionation (Young & Galy, 2004). Given the linear relationship in three-isotope space, we discuss only δ^{26}Mg values.

4. Results

Measured δ^{26}Mg and δ^{25}Mg values for the sample suite are presented in Table 1 and shown in Figure 2. The observed range for this study is ~4.6‰ (−3.4‰ to +1.2‰), or >60% of the observed variability in δ^{26}Mg values on Earth (~7.5‰, from −5.6‰ to +1.8‰; Teng, 2017), and include δ^{26}Mg values that are both higher than and lower than unaltered mantle peridotite.

Table 1
Samples Numbers, Reference, Lithology, Mg Isotopic Compositions, MgO, and SiO_2 wt%

Sample	Reference	Lithology	δ^{26}Mg	δ^{25}Mg	MgO wt%	SiO_2 wt%
OM94-99	Hanghøj et al. (2010)	Dunite	−0.22	−0.11	42.76	35.50
OM94-52D*	Hanghøj et al. (2010)	Dunite	−0.25	−0.11	39.84	32.92
OM94-74D	Hanghøj et al. (2010)	Dunite	−0.32	−0.15	44.41	36.77
OM94-110*	Hanghøj et al. (2010)	Dunite	−0.17	−0.06	41.70	37.79
OM94-67	Hanghøj et al. (2010)	Harzburgite	−0.25	−0.12	40.93	40.43
OM94-103	Hanghøj et al. (2010)	Harzburgite	−0.22	−0.11	41.39	42.22
OM94-61	Hanghøj et al. (2010)	Harzburgite	−0.24	−0.09	40.73	38.90
OM94-98	Hanghøj et al. (2010)	Harzburgite	−0.20	−0.09	41.38	41.30
OM94-101	Hanghøj et al. (2010)	Harzburgite	−0.29	−0.16	40.63	41.12
OM94-52H	Hanghøj et al. (2010)	Harzburgite	−0.42	−0.22	39.21	38.77
OM13-19	de Obeso and Kelemen (2018)	Harzburgite	−0.17	−0.09	39.65	38.86
OM13-2	de Obeso and Kelemen (2018)	Harzburgite	−0.24	−0.14	40.94	39.16
OM13-4	de Obeso and Kelemen (2018)	Dunite	−0.24	−0.09	28.29	31.97
OM15-5-4	de Obeso and Kelemen (2020)	Harzburgite	−0.10	−0.07	39.13	41.33
OM15-6-4	de Obeso and Kelemen (2020)	Harzburgite	−0.09	−0.03	39.96	43.56
OM15-7-4	de Obeso and Kelemen (2020)	Harzburgite	−0.09	−0.07	37.54	42.49
OM15-5-3	de Obeso and Kelemen (2020)	Oxidized harzburgite	0.94	0.49	29.18	39.99
OM15-6-3	de Obeso and Kelemen (2020)	Oxidized harzburgite	0.86	0.46	28.60	39.21
OM15-7-3	de Obeso and Kelemen (2020)	Oxidized harzburgite	0.77	0.41	28.00	38.18
OM15-5-2	de Obeso and Kelemen (2020)	Altered harzburgite	0.74	0.38	28.75	44.81
OM15-6-2	de Obeso and Kelemen (2020)	Altered harzburgite	0.74	0.40	29.08	45.54
OM15-7-2	de Obeso and Kelemen (2020)	Altered harzburgite	0.70	0.37	28.81	46.43
OM13-15A	This study	Serpentinite	0.17	0.08	38.23	35.28
OM15-5-5	This study	"Waxy" vein	1.19	0.60	46.04	32.05
OM13-15B	This study	Serpentine vein	0.45	0.20	40.74	37.32
OM13-17A WP	This study	Serpentine vein	0.96	0.51	41.44	40.28
OM09-11	Falk and Kelemen (2015)	Magnesite listvenite	−0.33	−0.18	30.53	27.75
OM10-26	Falk and Kelemen (2015)	Magnesite listvenite	−0.33	−0.16	26.03	34.57
OM10-14	Falk and Kelemen (2015)	Dolomite listvenite	−1.46	−0.78	16.35	12.30
OM10-15	Falk and Kelemen (2015)	Dolomite listvenite	−0.89	−0.48	10.72	24.93
OM07-39	Streit et al. (2012)	Massive magnesite vein	−3.14	−1.64	44.94	1.09
OM07-27	Streit et al. (2012)	Massive dolomite vein	−1.91	−1.02	21.78	7.82
OM17 magnesite	This study (1)	Massive magnesite vein	−3.38	−1.75	bdl	45.41
OM17 magnesite	This study (2)	Massive magnesite vein	−3.39	−1.76	bdl	45.41
OM17 magnesite	This study (3)	Massive magnesite vein	−3.38	−1.79	bdl	45.41
OM17 magnesite	This study (4)	Massive magnesite vein	−3.38	−1.78	bdl	45.41
OM17 magnesite	This study (5)	Massive magnesite vein	−3.36	−1.74	bdl	45.41
OM07-18	Kelemen et al. (2011) only mineralogy	Travertine forming now	−1.17	−0.58	2.29	1.80
OM07-18	Kelemen et al. (2011) only mineralogy (2)	Travertine forming now	−1.11	−0.56	2.29	1.80
OM07-34A	Kelemen et al. (2011) only mineralogy	Old travertine	−0.92	−0.44	3.12	2.5
OM07-34A	Kelemen et al. (2011) only mineralogy (2)	Old travertine	−0.87	−0.45	3.12	2.5
OM07-07	Kelemen et al. (2011) only mineralogy	Carbonate vein	−3.39	−1.75	47.27	na
BA1B 11-2 17–27 cm	This study from mineralogy	Huntite vein	−3.04	−1.57	34.25	na

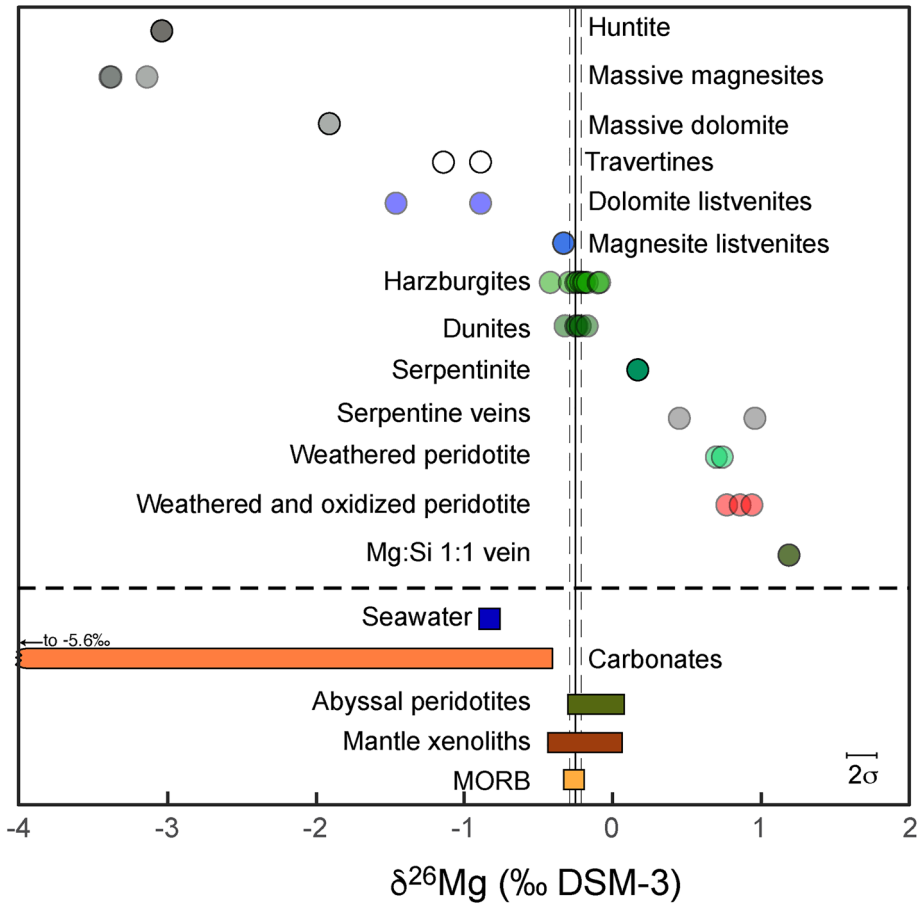

Figure 2. δ^{26}Mg for studied samples from the Oman ophiolite and selected terrestrial reservoirs (colored rectangles from Teng [2017]). Black solid line represents the average mantle value, and vertical dashed black lines delineate the range of variability of mantle compositions from Teng (2010, 2017). Earth δ^{26}Mg range is ~7.5‰ (Teng, 2017).

Measured δ^{26}Mg values in partially serpentinized harzburgites and dunites are indistinguishable from the mantle (−0.25 ± 0.14‰ (2σ) and −0.24 ± 0.10‰ (2σ), respectively, Figure 3). Three samples from Wadi Fins (OM15-5-4, OM15-6-4, and OM15-7-4; de Obeso & Kelemen, 2020) are characterized by average δ^{26}Mg values higher than the mantle (−0.09 ± 0.01‰, 2σ) are excluded from the harzburgite average as their compositions record significant Mg leaching (up to 30% in the most altered samples). Their completely hydrated (OM15-5-2, OM15-6-2, and OM15-7-2) and oxidized (OM15-5-3, OM15-6-3, and OM15-7-3) counterparts from the same outcrop are characterized by higher δ^{26}Mg values (average of +0.73 ± 0.04‰ for hydrated samples and +0.86 ± 0.17‰ for oxidized samples, 2σ) (Figure 2). Silicate mineral separates from veins in the Wadi Fins area are also characterized by δ^{26}Mg higher than the mantle. Two serpentine veins (OM13-17A WP and OM13-15B) have δ^{26}Mg values of +0.45‰ and +0.96‰ respectively, and a "waxy vein" (OM15-5-5) with molar Mg/Si of 1, composed of serpentine + stevensite or talc, has a δ^{26}Mg value of +1.19‰ (Figure 2).

Measured δ^{26}Mg values in two magnesite listvenites (OM09-11 and OM10-26) are identical and indistinguishable from mantle values (−0.33‰, Figure 2), suggesting nearly isochemical carbonation as inferred from major element ratios by Falk and Kelemen (2015). In contrast, two dolomite listvenites (OM10-14 and OM10-15) are characterized by lower δ^{26}Mg values, −1.46‰ and −0.89‰, respectively. Two massive magnesite veins (OM07-39, OM17 Magnesite) record δ^{26}Mg values of −3.14‰ and −3.39‰, or ~3‰ lower than the mantle. Dolomite (OM07-27) and huntite (BA1B 11-2 17–27cm) veins extracted from serpentinized peridotites are also characterized by low δ^{26}Mg values, −1.91‰ and −3.04‰, respectively. Finally, travertines with Mg-rich calcite (OM07-18 and OM07-34A) precipitated from Ca^{2+}-rich hyperalkaline springs (type II waters) are characterized by higher δ^{26}Mg than the other carbonates (−1.14‰ and −0.89‰).

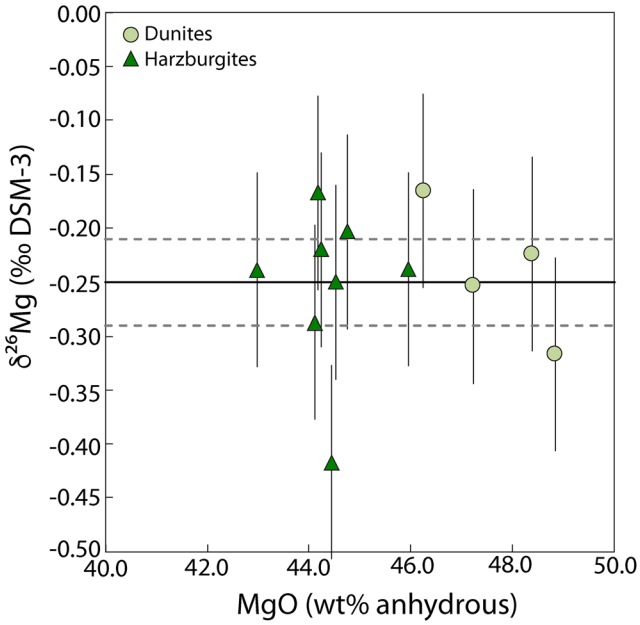

Figure 3. δ^{26}Mg (relative to DSM-3) vs. MgO (wt% anhydrous) for harzburgites and dunites. Black solid line represents the mantle average and dashed black lines encompass the range of mantle variability (Teng, 2017; Teng et al., 2010).

5. Discussion

5.1. δ^{26}Mg Changes Resulting From Magnesium Mobility

The degree of alteration of mantle peridotite can be assessed by looking at deviations from the mantle fractionation produced by melting and melt extraction in an MgO/SiO_2 vs. Al_2O_3/SiO_2 plot (Figure 4). The mantle fractionation trend is a linear fit to theoretical and observed residues of mantle melting and melt extraction during adiabatic decompression beneath oceanic spreading ridges (Asimow, 1999; Baker & Beckett, 1999; Jagoutz et al., 1979). Departures from the mantle fractionation trend due to alteration and weathering are reflected in deviation toward lower MgO/SiO_2 values. In Oman, it is estimated that typical partially serpentinized harzburgites might have lost up to 2 wt% MgO on average (Monnier et al., 2006), though in some cases Si gain can also lead to decreased MgO/SiO_2 ratios (de Obeso & Kelemen, 2018). Heavily weathered samples within 10 m of a Cretaceous unconformity in Wadi Fins lost 30% of their initial Mg to the alteration fluid (de Obeso & Kelemen, 2020) and laterites along this unconformity elsewhere in Oman have lost even larger proportions of magnesium (Al-Khirbash, 2016, 2015). Nearly isochemical serpentinization of peridotite (other than H_2O addition) should preserve the MgO/SiO_2 ratio of the original protolith, whereas deviations in all of our samples require Mg loss (Monnier et al., 2006; Snow & Dick, 1995) and/or Si-addition (de Obeso & Kelemen, 2018). This suggest that open system mass transfer of major elements has occurred during alteration (Figure 4).

Furthermore, the presence of meter-wide veins of magnesite in the Samail ophiolite mantle section provides additional evidence of Mg mobility (Figure 5). However, the veins alone do not indicate if the Mg is derived by minor leaching from a large mass of peridotite, or extensive leaching from a smaller mass. Most analyzed

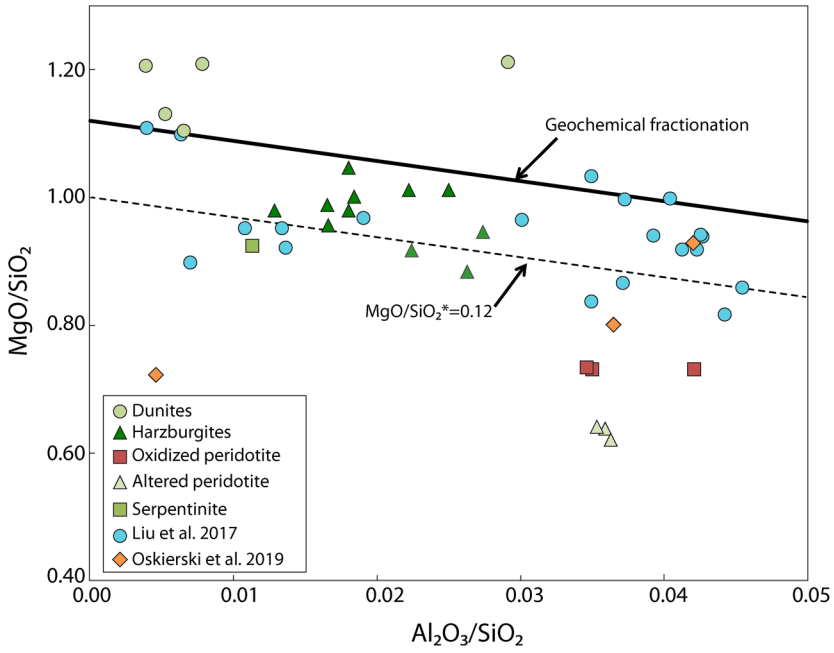

Figure 4. Whole rock MgO/SiO_2 vs Al_2O_3/SiO_2 showing sample deviations associated with peridotite alteration from the mantle fractionation trend (bold black line). The mantle fractionation trend is a linear fit to theoretical and observed residues of mantle melting and melt extraction during adiabatic decompression beneath oceanic spreading ridges (Asimow, 1999; Baker & Beckett, 1999). $MgO/SiO_2^* = 0.12$ shown as dashed black line (Equation 1).

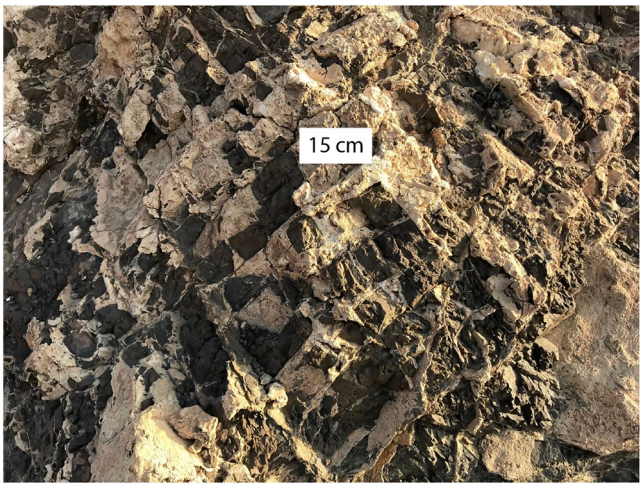

Figure 5. Massive magnesite veins containing angular blocks of serpentinized harzburgite in the Oman ophiolite (UTM 40Q E 671274 N 2536144).

magnesite, dolomite, and calcite veins in Samail ophiolite peridotites record measurable ^{14}C, corresponding to ages less than ~50 ka (Kelemen & Matter, 2008; Kelemen et al., 2011, 2019; Mervine et al., 2014; Streit et al., 2012), suggesting that some of the alteration associated with Mg mobility occurred in the Pleistocene and Holocene.

In order to account for serpentinized harzburgite departures from the geochemical fractionation trend (Asimow, 1999; Baker & Beckett, 1999) during alteration we use MgO/SiO_2* (Liu et al., 2017; Snow & Dick, 1995) defined as

$$\left(\frac{MgO}{SiO_2}\right)^* = \left(-3.15 * \left(\frac{Al_2O_3}{SiO_2}\right)_{sample} + 1.12\right) - \left(\frac{MgO}{SiO_2}\right)_{sample}. \quad (1)$$

MgO/SiO_2* is a measure of how altered a sample is, either from Mg loss (Liu et al., 2017; Snow & Dick, 1995) or Si gain (de Obeso & Kelemen, 2018). A sample with $MgO/SiO_2^* = 0$ plots along the geochemical fractionation line (Asimow, 1999; Baker & Beckett, 1999). Increasing MgO/SiO_2* correlates with higher degrees of alteration indicative of mass transfer.

All analyzed harzburgites in this study have $\left(\frac{MgO}{SiO_2}\right)^* > 0$ indicative of Mg loss (Snow & Dick, 1995) and/or Si-addition (de Obeso & Kelemen, 2018) (Figure 5). Samples with $\left(\frac{MgO}{SiO_2}\right)^* < 0.12$ are partially serpentinized harzburgites with $\delta^{26}Mg$ indistinguishable from the Earth's mantle and BSE ($\delta^{26}Mg = -0.25 \pm 0.04‰$; Teng, 2017). As $\left(\frac{MgO}{SiO_2}\right)^*$ increases, whole rocks begin to deviate to heavier Mg isotope ratios (Figure 6).

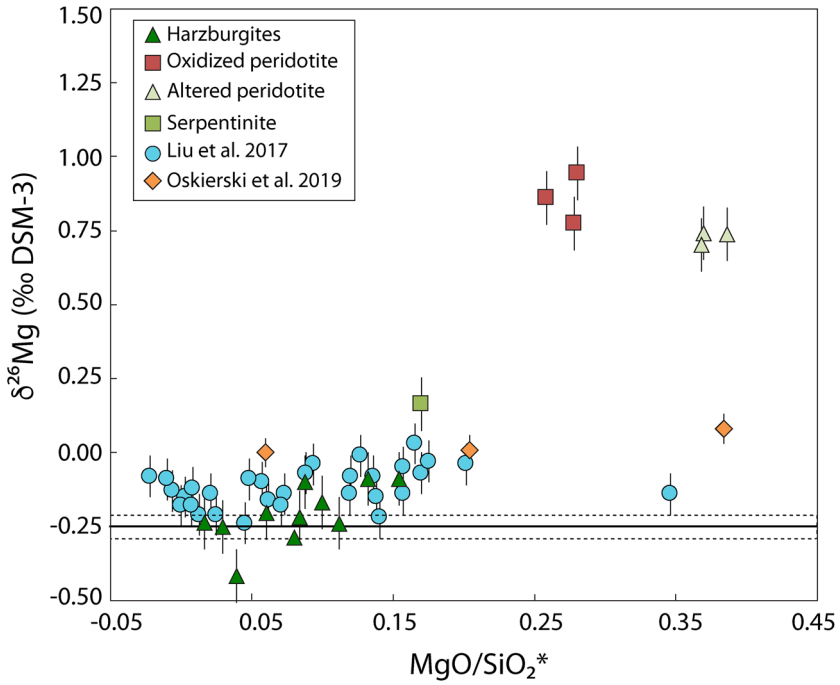

Figure 6. Bulk-rock MgO/SiO_2* vs. $\delta^{26}Mg$ for Oman samples, abyssal peridotites (Liu et al., 2017) and serpentinite (Oskierski et al., 2019). Black solid line is mantle average and dashed black lines delineate the range of variability of mantle compositions (Teng, 2017; Teng et al., 2010).

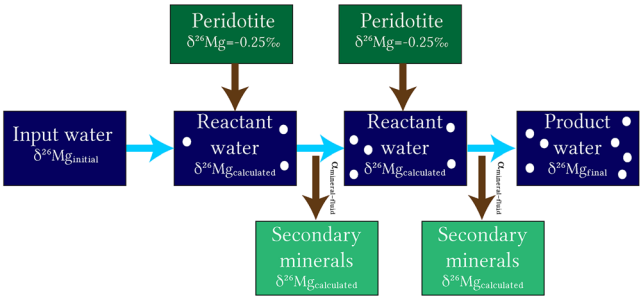

Figure 7. Schematic of fluid-centered flow model after Paukert et al. (2012).

Samples with the highest $\left(\frac{MgO}{SiO_2}\right)^*$ in this study are the most enriched in ^{26}Mg and contain Mg-rich clays (de Obeso & Kelemen, 2020). These deviations suggest that (1) variable amounts of Mg have been leached from the peridotites depending on the degree of alteration at different W/R and (2) small Mg depletions are not reflected in $\delta^{26}Mg$ of the partially serpentinized harzburgites, which retain mantle-like Mg even at high degrees of serpentinization (e.g., OM13-2 and OM13-19).

We associate the observed Mg mobility with the formation of alteration products in high W/R pathways, including serpentine and carbonates veins with $\delta^{26}Mg$ values that depart dramatically from the canonical mantle value. In particular, Mg-carbonates have $\delta^{26}Mg$ between −0.64‰ and −3.14‰ lower than unaltered peridotite. Serpentine veins from Wadi Fins are depleted in Fe (Mg# 97–98) compared to ambient peridotite (Mg# 90), and are interpreted to have formed at high water-to-rock ratios at temperatures between 25°C and 60°C (de Obeso & Kelemen, 2018). Measured $\delta^{26}Mg$ values of these serpentine veins are up to 1.2‰ higher than unaltered peridotite. Little or no Mg isotope fractionation, relative to mantle values, has been found in our whole rock samples of partially serpentinized peridotites, and in previous studies of similar lithologies (Beinlich et al., 2014; Liu et al., 2017). Thus, a different process for the formation of ^{26}Mg-enriched serpentine veins is required. Possibilities include (1) veins were enriched in ^{26}Mg due to isotopic fractionation associated with serpentine precipitation; (2) serpentine precipitated from a fluid enriched in ^{26}Mg due to the removal of ^{24}Mg in other alteration minerals (e.g., carbonates); or (3) some combination of (1) and (2).

5.2. Reaction Path Modeling

5.2.1. Model Setup

To explore the hypothesis that elevated $\delta^{26}Mg$ values in serpentine veins are largely the consequence of precipitation from a high $\delta^{26}Mg$ fluid, formed by previous fractionation during crystallization of low ^{26}Mg carbonates, we developed a simple reactive transport model that simulates dissolution of primary minerals together with fractional crystallization of serpentine and carbonates based on the reaction path outlined by Barnes and O'Neil (1969) for serpentinization and carbonation systems and modeled by subsequent workers (Bruni et al., 2002; Paukert et al., 2012). We used the Paukert et al. (2012) model that reproduces measured aqueous solute concentrations in the peridotite-hosted springs via water-rock interaction, including coprecipitation of carbonates and serpentine. Model is setup using fluid-centered flow-through physical system. The model follows the evolution of a parcel of water (1 kg) reacting with fresh peridotite and forming secondary minerals. The fresh peridotite reservoir is assumed to be unlimited and inputs into the system are controlled by the dissolution of primary minerals. After each reaction step precipitated secondary minerals are tallied and removed from the system so they cannot undergo further reactions. The evolved fluid moves to the next step and reacts with new peridotite. A conceptual view of the model is shown in Figure 7. $\delta^{26}Mg$ calculated is computed at each reaction step for fluid and secondary minerals. Most minerals associated with Mg mobility are modeled in the reaction path. This allows us to explore whether the evolution of Mg isotope compositions in alteration minerals during coprecipitation of carbonates and silicates is plausible and consistent with our data.

This model has three stages. In Stage I, rainwater in equilibrium with the atmosphere infiltrates the peridotite, forming chrysotile, calcite, hydromagnesite, and magnetite. The fluid formed in Stage I has an Mg^{2+}-HCO_3^- rich composition (Type I). In Stage II, Type I fluid reacts with fresh peridotite isolated from the atmosphere to form magnesium-rich carbonates, chrysotile, and brucite, with the fluid evolving to Ca^{2+}-OH^- rich, Mg^{2+}-HCO_3^- poor compositions (Type II) until pH reaches 12 (maximum pH measured in the field). In Stage III (not explicitly modeled by Paukert et al. [2012]), Type II fluids emerge on the surface and react with atmospheric CO_2 to form calcite. The model tracks the evolution of $\delta^{26}Mg$ in the resulting fluid and precipitated minerals during each stage. Important model variables and relevant references are given

Table 2
Model Parameters

Model parameter	Value	Reference
Temperature	30°C	Weyhenmeyer et al. (2002)
Magnesite $\alpha_{mgs\text{-}fluid}$	0.9972	Wang et al. (2019)
	0.9954	Schauble et al. (2011)
	0.9979	Schott et al. (2016)[a]
Dolomite $\alpha_{dol\text{-}fluid}$	0.9981	Wang et al. (2019)
	0.9965	Schauble et al. (2011)
	0.9983	Li et al. (2015)
Hydromagnesite $\alpha_{hmgs\text{-}fluid}$	0.9990	Shirokova et al. (2013)
Initial δ^{26}Mg fluid	−2.0‰	Teng (2017)
$[Mg]_0$ fluid	7.7×10^{-5} molal	Paukert et al. (2012)
Peridotite δ^{26}Mg	−0.25‰	Teng (2017)
[Mg] peridotite	28.4 wt%	Paukert et al. (2012)

[a]Schott is extrapolated from batch reaction data.

in Table 2. They include initial δ^{26}Mg fluid compositions, $Mg_{mineral\text{-}fluid}$ fractionation factors (α), and the temperature of alteration.

Equilibrium isotope fractionation of Mg isotopes is temperature dependent (Li et al., 2015; Pinilla et al., 2015; Ryu et al., 2016; Schott et al., 2016; Wang et al., 2019), rendering temperature estimates important for understanding alteration. For calculations in this study, we used 30°C, approximately the current annual average temperature in the northern Oman mountains (Weyhenmeyer et al., 2002). This temperature is consistent with other constraints established in studies of most of the samples analyzed in this study. de Obeso and Kelemen (2018) estimated that alteration in Wadi Fins occurred between 25°C and 60°C based on clumped isotope thermometry of carbonate veins in peridotite. Carbonate veins in typical, partially serpentinized mantle peridotites in the Samail ophiolite also yield crystallization temperatures between 25°C and 50°C, calculated using both δ^{18}O exchange and clumped isotope thermometry (Kelemen et al., 2011; Streit et al., 2012).

Our model assumes that products of nearly isochemical, olivine serpentinization do not fractionate Mg isotopes from the fluid ($\alpha = 1.0000$ for serpentine and brucite) as concluded in previous studies of natural samples (Beinlich et al., 2014; Liu et al., 2017). The preferential incorporation of ^{24}Mg in carbonates, reported both in experimental and field observations (Higgins & Schrag, 2010; Li et al., 2015; Mavromatis et al., 2013; Pearce et al., 2012; Shirokova et al., 2013; Tipper et al., 2006), is a critical factor in our model. This isotopic fractionation is largely responsible for producing the fluid with high δ^{26}Mg that then produces serpentine veins with heavy Mg. We used carbonate-fluid fractionation factors (α) from empirical and experimental studies. For hydromagnesite, we used a fractionation factor of $\alpha = 0.9990$, derived from low-temperature precipitation experiments using alkaline natural water of Salda Lake, Turkey (Shirokova et al., 2013). We prefer this value to the only other published value for hydromagnesite (Oelkers et al., 2018), because the latter group attributed their results to disequilibrium processes. For magnesite and dolomite, we used a range of fractionation factors reported in the literature, as listed in Table 2. Precipitation kinetics of magnesite and dolomite at low temperatures are poorly understood (Arvidson & Mackenzie, 1999; Saldi et al., 2012). Dolomite crystallization has not been achieved in laboratory conditions, even after a 3 decade long experiment (Land, 1998), and until 2017 magnesite had not been experimentally crystallized at temperatures below 60°C (e.g., Hänchen et al., 2008; Johnson et al., 2014), though more recent work produced magnesite at room temperature from fluids enriched in organic ligands (Power et al., 2017). In our models, magnesite-water fractionation factors at 30°C were extrapolated from higher temperature experiments (Li et al., 2015; Schott et al., 2016) or derived from first principles estimates and molecular dynamics (Schauble, 2011; Wang et al., 2019). Mg fractionation between calcite and fluid depends on multiple factors in

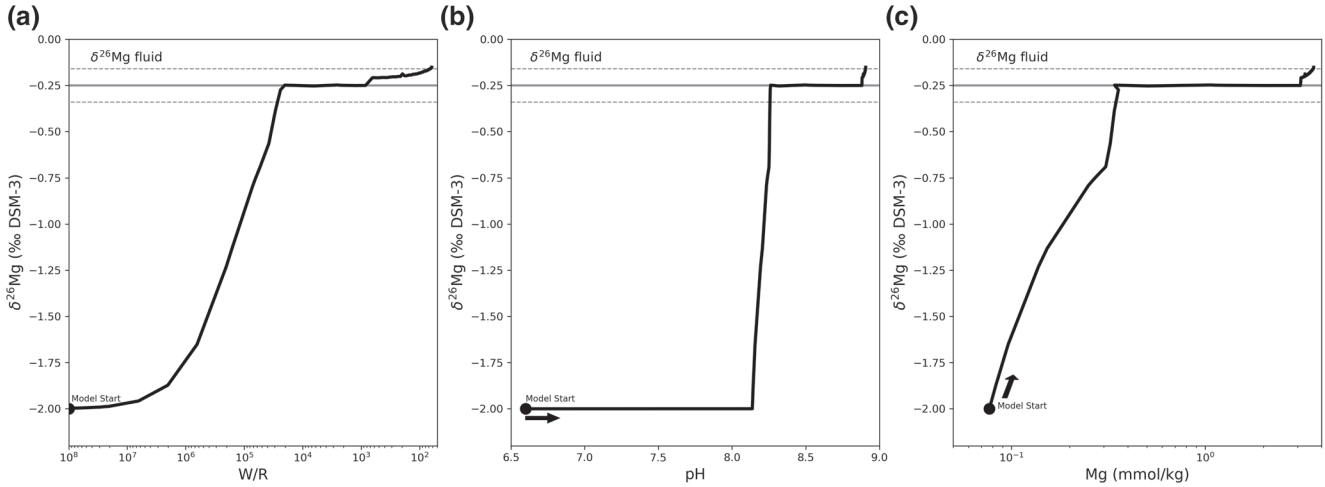

Figure 8. δ^{26}Mg evolution of the fluid in the first stage of reaction, open to gas exchange with the atmosphere as a function of W/R (a), pH (b), and Mg molality (c), reaction progress is from left to right as marked with black arrows. Black solid line is mantle average and dashed black lines delineate the range of variability of mantle compositions (Teng, 2017; Teng et al., 2010).

addition to temperature (Li et al., 2012), including Mg content (Wang et al., 2019) and precipitation rate (Mavromatis et al., 2013). Considered these factors and as calcite is only a minor player in the system Mg budget (<0.1% by weight) it is not considered in the model.

The first two stages of the reaction path model yield calculated Mg isotope compositions of the fluid and precipitated minerals as a function of pH and water/rock ratio (W/R) calculated as remaining water in the system/reacted rock by mass. We used the fractionation factors described above, and a model of assimilation and fractional crystallization (AFC) (DePaolo, 1981), as the system is similar to a magmatic system where water assimilate peridotite and fractionally crystalize secondary minerals. The primary minerals (olivine, orthopyroxene, and clinopyroxene) in the model have δ^{26}Mg of −0.25‰. At each step of the model, primary minerals are dissolved and secondary minerals (chrysotile + hydromagnesite in Stage I, chrysotile + brucite + dolomite and magnesite in Stage II) are allowed to precipitate. The shallow aquifer that represents the first stage fluids are recharged by rainwater contaminated with limestone dust (Paukert et al., 2012) so we assume that the starting Mg isotope composition of this fluid is in equilibrium with the late Cretaceous to Eocene limestones that locally overlie the ophiolite. For this we use the global average of limestones δ^{26}Mg (Teng, 2017) using $\Delta^{26}Mg_{\text{limestone-fluid}} = 2‰$ resulting in an initial $\delta^{26}Mg_{\text{fluid}}$ of −2.0‰, similar to δ^{26}Mg values of riverine water in limestone catchments (Tipper et al., 2006). Values for $\delta^{26}Mg_{\text{fluid}}$ at each model step are calculated using the AFC equation (DePaolo, 1981) for stable isotopes:

$$\delta_f - \delta_f^0 = \left(\frac{r}{r-1}\right)\frac{C_a}{zC_f}\left[\delta_a - \delta_f^0 - \frac{D\Delta}{z(r-1)}\right]X\left(1-F^{-z}\right) - \frac{D\Delta}{(r-1)}\ln F\left[1-\left(\frac{r}{r-1}\right)\frac{C_a}{zC_f}\right], \quad (2)$$

where δ_f and δ_a are the δ^{26}Mg of the fluid and the primary minerals, respectively, $\Delta = 1{,}000\ \ln\alpha_{\text{mineral-fluid}}$, r is the ratio of mass assimilated over mass precipitated, D is the bulk partition coefficient between secondary minerals and fluid, C_f is the Mg concentration in the fluid, C_a is the Mg concentration in the primary minerals, $z = (r + D - 1)/(r - 1)$ and F is the ratio of fluid mass to initial fluid mass available to bound to secondary minerals. δ^{26}Mg of secondary minerals is calculated in each step using the fluid Mg isotope compositions and precipitated minerals fractionation factors ($\alpha_{\text{mineral-fluid}}$).

5.2.2. Model Results

In Stage I, small extents of water-rock interaction (high W/R) cause fluid evolution from the initial δ^{26}Mg of −2‰ to a value of −0.25‰ (Figure 8a) as the dissolved Mg^{2+} concentration in the fluid increases and

becomes dominated by input from dissolution of primary minerals. This evolution in δ^{26}Mg occurs together with a drastic increase in pH from its initial value of 6.6–~8.2 (Figure 8b). The evolved fluid has higher final concentrations of Mg (Figure 8c) and HCO_3 and becomes slightly enriched in heavy isotopes (δ^{26}Mg = −0.15‰) when it gets saturated in hydromagnesite at [Mg] ~ 3.4 mmol/kg, pH ~ 8.9 at W/R less than 1,000.

In Stage II, the Mg-HCO_3 rich fluid evolves to Mg-depleted and C-depleted waters with high Ca^{2+} and pH as well as extremely low fO_2. Mineral precipitation is dominated by formation of magnesite and chrysotile with minor dolomite, at W/R between 2,000 and 100,000, and constant pH of 7.9 (Figures 9a and 9b). Mg-rich carbonates begin to precipitate with their lowest δ^{26}Mg values, and evolve to heavier compositions as W/R decreases (Figures 9e and 9g) and pH increases after an initial decrease with only serpentine forming (Figures 9d, 9f, and 9h). The precipitation of Mg-rich carbonates drives fluid and serpentine to higher δ^{26}Mg (Figures 9c and 9d) with the highest achieved at the lowest pH (Figure 9d). Once the system becomes carbon-depleted, and magnesite disappears from the crystallizing mineral assemblage at W/R ~ 1,800 and pH 9.8, the fluid/serpentine system rapidly evolves to mantle-like isotope ratios (Figures 9c and 9d) with dolomite disappearing from the system but in amounts not impacting δ^{26}Mg (Figures 9g and 9h).

Given the range of model variables listed in Table 2, our model does not capture the absolute values measured in our samples although it is able to explain three aspects of our Mg isotope data: (1) low δ^{26}Mg in massive carbonate veins, (2) high δ^{26}Mg in serpentine veins and some heavily weathered bulk-rock samples, and (3) δ^{26}Mg of partially altered ultramafic rocks that are indistinguishable from mantle values. The low-values reflect coprecipitation of serpentine and carbonate at high W/R ratios. As W/R decreases, carbonates disappear from the crystallizing assemblage, the fluid evolves to δ^{26}Mg = –0.25‰, and precipitated serpentine also has mantle-like Mg isotope ratios, consistent with observed values in this and other studies (Beinlich et al., 2014; Liu et al., 2017). Although the carbonate and serpentine samples in this study come from a broad region, and are not specifically cogenetic, our measurements and modeling show how serpentine veins can have magnesium isotopic ratios different from those of the protolith, even when serpentine-water exchange itself does not fractionate Mg isotopes.

In the natural system, the Type II hyperalkaline Ca-rich fluid comes in contact with the atmosphere in springs, where it combines with CO_2 from air to form extensive travertine deposits (Chavagnac et al., 2013a; Clark & Fontes, 1990; Kelemen & Matter, 2008; Kelemen et al., 2011; Mervine et al., 2014; Neal & Stanger, 1985). Travertines analyzed in this study have δ^{26}Mg of −1.14‰ and −0.89‰. In our modeling, at pH 12, the fluid has an isotope ratio identical to mantle values, δ^{26}Mg = −0.25‰. If calcite in travertines precipitated from this fluid, then the inferred $\Delta^{26}Mg_{cal\text{-}fl}$ of the travertine must have been lower than the value of ~3‰ expected for equilibrium fractionation with such a fluid (Li et al., 2012; Mavromatis et al., 2017; Wang et al., 2019). Indeed, Mavromatis et al. (2013) showed that $\Delta^{26}Mg_{cal\text{-}fl}$ is dependent on the growth rate of calcite, with $\Delta^{26}Mg_{cal\text{-}fl} = (\delta^{26}Mg_{cal} - \delta^{26}Mg_{fl})$ decreasing with increasing growth rate. (This type of growth rate dependence has not been reported for magnesite or dolomite.) Extrapolating from Mavromatis et al. (2013) best-fit correlation the inferred $\Delta^{26}Mg_{cal\text{-}fl}$ for calcite in Oman travertines suggests calcite growth rates between $10^{-5.4}$ and $10^{-4.7}$ mol/(m^2 s). Such rapid growth is consistent with the nonequilibrium, high Mg contents in peridotite-hosted travertines in the Samail ophiolite and other massifs (e.g., Barnes & O'Neil, 1971, 1969; Chavagnac et al., 2013; Kelemen & Matter, 2008; Kelemen et al., 2011; Streit et al., 2012). Assuming that 1–10% of the total estimated travertine area in the Samail ophiolite (~10^7 m^2 (Kelemen & Matter, 2008)) is actively precipitating, this rate yields a total uptake of 10^3–10^4 tons atmospheric CO_2/yr, similar to previous estimates of surface carbon uptake to form travertine in the ophiolite (Kelemen & Matter, 2008; Kelemen et al., 2011; Mervine et al., 2014), as shown schematically in Figure 10.

6. Conclusions

Most partially serpentinized dunites and harzburgites in the mantle section of the Samail ophiolite have δ^{26}Mg indistinguishable from average mantle values. Serpentinization at low W/R does not fractionate Mg isotopes. However, deviations from mantle δ^{26}Mg are observed in rocks which have undergone extensive Mg leaching at higher W/R. Heavily altered peridotites recording up to 30% Mg loss, and containing Mg-clay minerals, have the heaviest δ^{26}Mg ever reported for ultramafic rocks. We model a mechanism in which

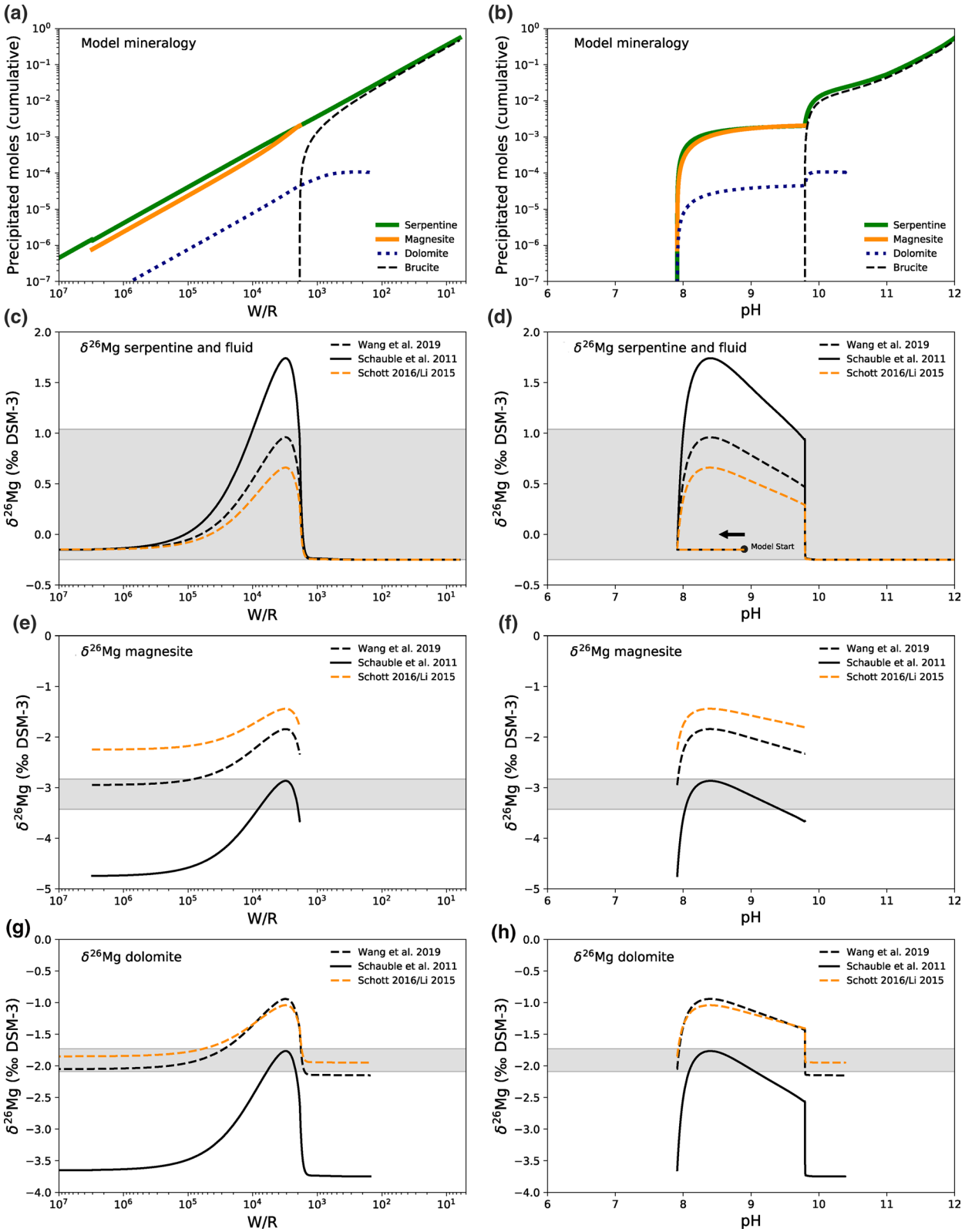

Figure 9. Results from the second stage of the reaction path model, closed to exchange with the atmosphere as a function of W/R and pH, illustrating mineral products (a and b), δ^{26}Mg of fluid and serpentine (c and d), magnesite (e and f), and dolomite (g and h) using different fractionation factors from Wang et al. (2019), Shauble et al. (2011), Schott et al. (2016), and Li et al. (2015). Gray squares illustrate the observed range of sample values for each mineral. Reaction progress goes generally from left to right except in Figure 9d where arrow illustrates reaction progress direction and dot initial start point.

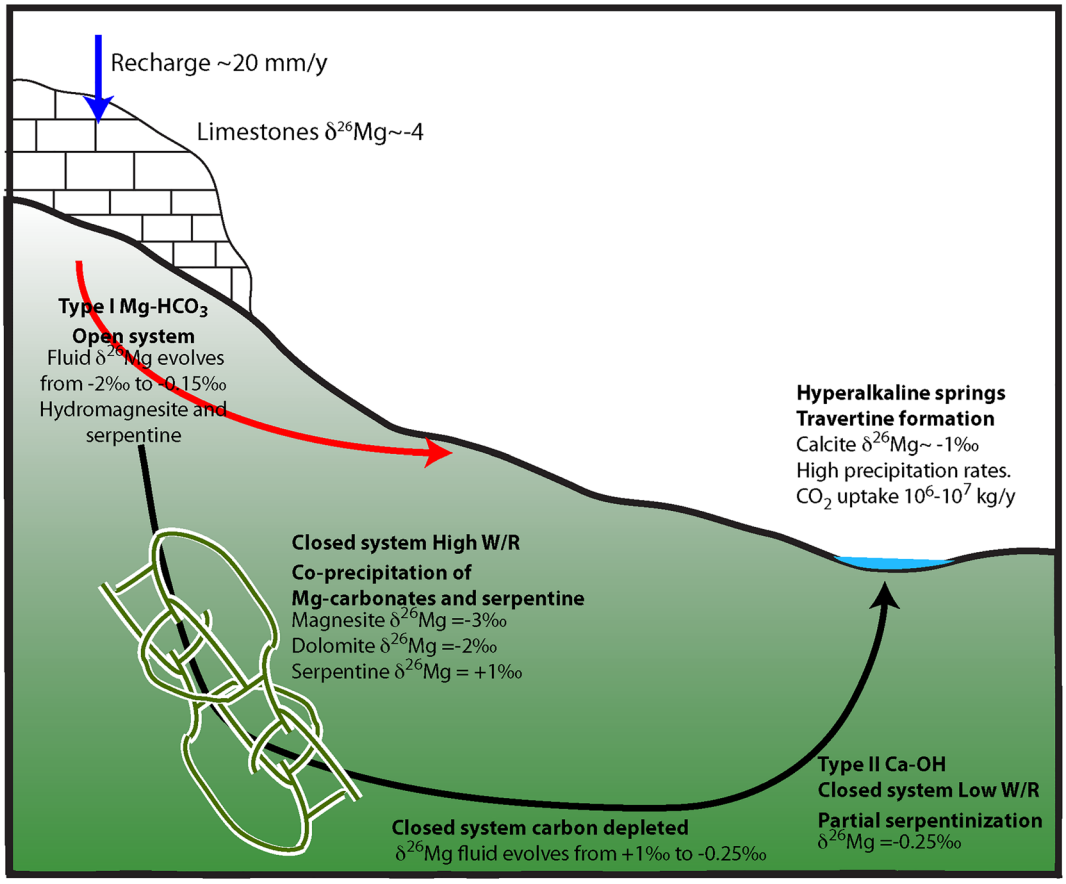

Figure 10. Conceptual model of Mg isotope systematics in the modern alteration system in Oman (after Dewandel et al., 2005; Neal & Stanger, 1985).

Mg-rich carbonates precipitate at high W/R, preferentially incorporating ^{24}Mg and producing ^{26}Mg-rich fluids that then precipitate serpentine veins with heavy Mg. When carbonates disappear from the crystallizing assemblage at lower W/R, serpentine evolves to mantle-like δ^{26}Mg. The modeled δ^{26}Mg for serpentine formed along with carbonates is similar to observed δ^{26}Mg in serpentine vein samples and although does not capture the absolute values perfectly it explains the trend observed in the samples. The fact that most peridotite-hosted carbonate veins have finite ^{14}C ages, along with our modeling results, is consistent with other observations indicating that serpentinization and carbonation are ongoing in the mantle section of the Oman ophiolite. The proposed mechanism can be further explored using cogenetic carbonate-serpentine veins from the newly drilled cores from the Oman Drilling Project and fluids from boreholes and/or springs. δ^{26}Mg in calcite forming travertine deposits at peridotite-hosted alkaline springs is heavier than expected from equilibrium fractionation between calcite and fluid with mantle-like Mg isotope ratios, suggesting rapid, disequilibrium crystallization. We infer calcite growth rates of 10^{-5} mol/m^{2}s, corresponding to uptake of atmospheric CO_2 at a rate of 10^6–10^7 kg CO_2/yr to form travertine in Oman.

Data Availability Statement

All new geochemical data for this work are available in the EarthChem Library at https://doi.org/10.26022/IEDA/111748 and https://doi.org/10.26022/IEDA/111749.

Acknowledgments
We thank everyone at the Sultanate of Oman Public Authority for Mining, especially Dr. Ali Al Rajhi for facilitating our fieldwork in Oman. We thank editor Stephen Parman and an anonymous associate editor for editorial handling of this manuscript. Reviews from Ed Tipper, Christopher Pearce and an anonymous reviewer helped to greatly improve the manuscript. This work was supported through the Sloan Foundation–Deep Carbon Observatory (Grant 2014-3-01, Kelemen PI), the U.S.-National Science Foundation (NSF-EAR-1516300, Kelemen lead PI).

References

Al-Khirbash, S. (2015). Genesis and mineralogical classification of Ni-laterites, Oman Mountains. *Ore Geology Reviews*, *65*, 199–212. https://doi.org/10.1016/j.oregeorev.2014.09.022

Al-Khirbash, S. (2016). Geology, mineralogy, and geochemistry of low grade Ni-lateritic soil (Oman Mountains, Oman). *Geochemistry*, *76*(3), 363–381. https://doi.org/10.1016/j.chemer.2016.08.002

Arvidson, R. S., & Mackenzie, F. T. (1999). The dolomite problem; control of precipitation kinetics by temperature and saturation state. *American Journal of Science*, *299*, 257–288. https://doi.org/10.2475/ajs.299.4.257

Asimow, P. D. (1999). A model that reconciles major- and trace-element data from abyssal peridotites. *Earth and Planetary Science Letters*, *169*, 303–319. https://doi.org/10.1016/S0012-821X(99)00084-9

Auclair, M., Gauthier, M., Trottier, J., Jebrak, M., & Chartrand, F. (1993). Mineralogy, geochemistry, and paragenesis of the eastern metals serpentinite-associated Ni-Cu-Zn deposit, Quebec Appalachians. *Economic Geology*, *88*, 123–138. https://doi.org/10.2113/gsecongeo.88.1.123

Baker, M. B., & Beckett, J. R. (1999). The origin of abyssal peridotites: A reinterpretation of constraints based on primary bulk compositions. *Earth and Planetary Science Letters*, *171*, 49–61. https://doi.org/10.1016/S0012-821X(99)00130-2

Barnes, I., LaMarche, V. C., & Himmelberg, G. (1967). Geochemical evidence of present-day serpentinization. *Science*, *156*, 830–832. https://doi.org/10.1126/science.156.3776.830

Barnes, I., & O'Neil, J. R. (1969). The relationship between fluids in some fresh Alpine-type ultramafics and possible modern serpentinization, Western United States. *The Geological Society of America Bulletin*, *80*, 1947. https://doi.org/10.1130/0016-7606(1969)80[1947:TRBFIS]2.0.CO;2

Barnes, I., & O'Neil, J. R. (1971). Calcium-magnesium carbonate solid solutions from Holocene conglomerate cements and travertines in the Coast Range of California. *Geochimica et Cosmochimica Acta*, *35*, 699–718. https://doi.org/10.1016/0016-7037(71)90068-8

Barnes, I., O'Neil, J. R., & Trescases, J. (1978). Present day serpentinization in New Caledonia, Oman and Yugoslavia. *Geochimica et Cosmochimica Acta*, *42*, 144–145. https://doi.org/10.1016/0016-7037(78)90225-9

Beinlich, A., Austrheim, H., Mavromatis, V., Grguric, B., Putnis, C. V., & Putnis, A. (2018). Peridotite weathering is the missing ingredient of Earth's continental crust composition. *Nature Communications*, *9*, 634. https://doi.org/10.1038/s41467-018-03039-9

Beinlich, A., Mavromatis, V., Austrheim, H., & Oelkers, E. H. (2014). Inter-mineral Mg isotope fractionation during hydrothermal ultramafic rock alteration—Implications for the global Mg-cycle. *Earth and Planetary Science Letters*, *392*, 166–176. https://doi.org/10.1016/j.epsl.2014.02.028

Boudier, F., & Coleman, R. G. (1981). Cross section through the peridotite in the Samail ophiolite, southeastern Oman Mountains. *Journal of Geophysical Research*, *86*, 2573–2592.

Braun, M. G. (2004). *Petrologic and microstructural constraints on focused melt transport in dunites and rheology of the shallow mantle.*. WHOI/MIT.

Braun, M. G., & Kelemen, P. B. (2002). Dunite distribution in the Oman ophiolite: Implications for melt flux through porous dunite conduits. *Geochemistry, Geophysics, Geosystems*, *3*(11), 8603. https://doi.org/10.1029/2001GC000289

Bruni, J., Canepa, M., Chiodini, G., Cioni, R., Cipolli, F., Longinelli, A., et al. (2002). Irreversible water–rock mass transfer accompanying the generation of the neutral, Mg–HCO_3 and high-pH, Ca–OH spring waters of the Genova province, Italy. *Applied Geochemistry*, *17*, 455–474. https://doi.org/10.1016/S0883-2927(01)00113-5

Chavagnac, V., Ceuleneer, G., Monnin, C., Lansac, B., Hoareau, G., & Boulart, C. (2013a). Mineralogical assemblages forming at hyperalkaline warm springs hosted on ultramafic rocks: A case study of Oman and Ligurian ophiolites. *Geochemistry, Geophysics, Geosystems*, *14*, 2474–2495. https://doi.org/10.1002/ggge.20146

Chavagnac, V., Monnin, C., Ceuleneer, G., Boulart, C., & Hoareau, G. (2013b). Characterization of hyperalkaline fluids produced by low-temperature serpentinization of mantle peridotites in the Oman and Ligurian ophiolites. *Geochemistry, Geophysics, Geosystems*, *14*, 2496–2522. https://doi.org/10.1002/ggge.20147

Clark, I. D., & Fontes, J.-C. (1990). Paleoclimatic reconstruction in northern Oman based on carbonates from hyperalkaline groundwaters. *Quaternary Research*, *33*, 320–336. https://doi.org/10.1016/0033-5894(90)90059-T

Coleman, R. G., & Keith, T. E. (1971). A chemical study of serpentinization—Burro Moutain, California. *Journal of Petrology*, *12*, 311–328.

Collier, M. L. (2012). *Spatial-statistical properties of geochemical variability as constraints on magma transport and evolution processes at ocean ridges*. Columbia University.

de Obeso, J. C., & Kelemen, P. B. (2018). Fluid rock interactions on residual mantle peridotites overlain by shallow oceanic limestones: Insights from Wadi Fins, Sultanate of Oman. *Chemical Geology*, *498*, 139–149. https://doi.org/10.1016/J.CHEMGEO.2018.09.022

de Obeso, J. C., & Kelemen, P. B. (2020). Major element mobility during serpentinization, oxidation and weathering of mantle peridotite at low temperatures. *Philosophical Transactions. Series A, Mathematical, Physical, and Engineering Sciences*, *378*, 20180433. https://doi.org/10.1098/rsta.2018.0433

DePaolo, D. J. (1981). Trace element and isotopic effects of combined wallrock assimilation and fractional crystallization. *Earth and Planetary Science Letters*, *53*, 189–202. https://doi.org/10.1016/0012-821X(81)90153-9

Dewandel, B., Lachassagne, P., Boudier, F., Al-Hattali, S., Ladouche, B., Pinault, J. L., & Al-Suleimani, Z. (2005). A conceptual hydrogeological model of ophiolite hard-rock aquifers in Oman based on a multiscale and a multidisciplinary approach. *Hydrogeology Journal*, *13*, 708–726. https://doi.org/10.1007/s10040-005-0449-2

Esteban Guzman, J., Cuevas Urionabarrenechea, J., Tubía Martínez, J., Velasco Roldán, F., & Vegas Tubia, N. (2011). Características petrográficas y mineralógicas de birbiritas derivadas de las peridotitas de Ronda (Cordilleras Béticas). *Geogaceta*, *50*, 39–42.

Falk, E. S., & Kelemen, P. B. (2015). Geochemistry and petrology of listvenite in the Samail ophiolite, Sultanate of Oman: Complete carbonation of peridotite during ophiolite emplacement. *Geochimica et Cosmochimica Acta*, *160*, 70–90. https://doi.org/10.1016/j.gca.2015.03.014

Frost, R. B. (1985). On the stability of sulfides, oxides, and native metals in serpentinite. *Journal of Petrology*, *26*, 31–63. https://doi.org/10.1093/petrology/26.1.31

Galy, A., Belshaw, N. S., Halicz, L., & O'Nions, R. K. (2001). High-precision measurement of magnesium isotopes by multiple-collector inductively coupled plasma mass spectrometry. *International Journal of Mass Spectrometry*, *208*, 89–98. https://doi.org/10.1016/S1387-3806(01)00380-3

Galy, A., Yoffe, O., Janney, P. E., Williams, R. W., Cloquet, C., Alard, O., et al. (2003). Magnesium isotope heterogeneity of the isotopic standard SRM980 and new reference materials for magnesium-isotope-ratio measurements. *Journal of Analytical Atomic Spectrometry*, *18*, 1352–1356. https://doi.org/10.1039/B309273A

Gao, C., Cao, X., Liu, Q., Yang, Y., Zhang, S., He, Y., et al. (2018). Theoretical calculation of equilibrium Mg isotope fractionations between minerals and aqueous solutions. *Chemical Geology*, *488*, 62–75. https://doi.org/10.1016/J.CHEMGEO.2018.04.005

Godard, M., Jousselin, D., & Bodinier, J.-L. (2000). Relationships between geochemistry and structure beneath a palaeo-spreading centre: A study of the mantle section in the Oman ophiolite. *Earth and Planetary Science Letters*, *180*, 133–148. https://doi.org/10.1016/S0012-821X(00)00149-7

Gregory, R. T., & Taylor, H. P. (1981). An oxygen isotope profile in a section of cretaceous oceanic crust, Samail Ophiolite, Oman: Evidence for $\delta^{18}O$ buffering of the oceans circulation at mid-ocean ridges. *Journal of Geophysical Research*, *86*, 2737–2755.

Hänchen, M., Prigiobbe, V., Baciocchi, R., & Mazzotti, M. (2008). Precipitation in the Mg-carbonate system—Effects of temperature and CO_2 pressure. *Chemical Engineering Science*, *63*, 1012–1028. https://doi.org/10.1016/J.CES.2007.09.052

Hanghøj, K., Kelemen, P. B., Hassler, D., & Godard, M. (2010). Composition and genesis of depleted mantle peridotites from the Wadi Tayin Massif, Oman ophiolite; major and trace element geochemistry, and Os isotope and PGE systematics. *Journal of Petrology*, *51*, 201–227. https://doi.org/10.1093/petrology/egp077

Higgins, J. A., & Schrag, D. P. (2010). Constraining magnesium cycling in marine sediments using magnesium isotopes. *Geochimica et Cosmochimica Acta*, *74*, 5039–5053. https://doi.org/10.1016/j.gca.2010.05.019

Hindshaw, R. S., Tosca, R., Tosca, N. J., & Tipper, E. T. (2020). Experimental constraints on Mg isotope fractionation during clay formation: Implications for the global biogeochemical cycle of Mg. *Earth and Planetary Science Letters*, *531*, 115980. https://doi.org/10.1016/j.epsl.2019.115980

Hotz, P. E. (1964). Nickeliferous laterites in southwestern Oregon and northwestern California. *Economic Geology*, *59*, 355–396. https://doi.org/10.2113/gsecongeo.59.3.355

Husson, J. M., Higgins, J. A., Maloof, A. C., & Schoene, B. (2015). Ca and Mg isotope constraints on the origin of Earth's deepest $\delta^{13}C$ excursion. *Geochimica et Cosmochimica Acta*, *160*, 243–266. https://doi.org/10.1016/j.gca.2015.03.012

Jagoutz, E., Palme, H., Baddenhausen, H., Blum, K., Cendales, M., Dreibus, G., et al. (1979). The abundances of major, minor and trace elements in the earth's mantle as derived from primitive ultramafic nodules. In *Proceedings of the Lunar and Planetary Science Conference* (Vol. *10*. pp. 2031–2050).

Johnson, N. C., Thomas, B., Maher, K., Rosenbauer, R. J., Bird, D., & Brown, G. E. (2014). Olivine dissolution and carbonation under conditions relevant for in situ carbon storage. *Chemical Geology*, *373*, 93–105. https://doi.org/10.1016/J.CHEMGEO.2014.02.026

Kelemen, P. B., de Obeso, J. C., Manning, C., Godard, M., Bach, W., Cai, Y., et al. (2019). Peridotite alteration in OmanDP cores. *Geophysical Research Abstracts,* EGU2019–17259.

Kelemen, P. B., & Matter, J. M. (2008). In situ carbonation of peridotite for CO_2 storage. *Proceedings of the National Academy of Sciences of the United States of America*, *105*, 17295–17300. https://doi.org/10.1073/pnas.0805794105

Kelemen, P. B., Matter, J. M., Streit, E. E., Rudge, J. F., Curry, W. B., & Blusztajn, J. (2011). Rates and mechanisms of mineral carbonation in peridotite: Natural processes and recipes for enhanced, in situ CO_2 capture and storage. *Annual Review of Earth and Planetary Sciences*, *39*, 545–576. https://doi.org/10.1146/annurev-earth-092010-152509

Kelemen, P. B., Matter, J. M., Teagle, D. A. H., & Coggon, J. A. (Eds.) (2020). Proceedings of the Oman drilling project. *Proceedings of the International Ocean Discovery Program*. International Ocean Discovery Program. https://doi.org/10.14379/OmanDP.proc.2020

Land, L. (1998). Failure to precipitate dolomite at 25°C from dilute solution despite 1000-fold oversaturation after 32 years. *Aquatic Geochemistry*, *4*, 361–368.

Li, W., Beard, B. L., Li, C., Xu, H., & Johnson, C. M. (2015). Experimental calibration of Mg isotope fractionation between dolomite and aqueous solution and its geological implications. *Geochimica et Cosmochimica Acta*, *157*, 164–181.

Li, W., Chakraborty, S., Beard, B. L., Romanek, C. S., & Johnson, C. M. (2012). Magnesium isotope fractionation during precipitation of inorganic calcite under laboratory conditions. *Earth and Planetary Science Letters*, *333–334*, 304–316. https://doi.org/10.1016/J.EPSL.2012.04.010

Liu, P.-P., Teng, F.-Z., Dick, H. J. B., Zhou, M.-F., & Chung, S.-L. (2017). Magnesium isotopic composition of the oceanic mantle and oceanic Mg cycling. *Geochimica et Cosmochimica Acta*, *206*, 151–165. https://doi.org/10.1016/j.gca.2017.02.016

Lorand, J. P. (1988). Fe–Ni–Cu sulfides in tectonite peridotites from the Maqsad district, Sumail ophiolite, southern Oman: Implications for the origin of the sulfide component in the oceanic upper mantle. *Tectonophysics*, *151*, 57–73. https://doi.org/10.1016/0040-1951(88)90240-5

Malvoisin, B. (2015). Mass transfer in the oceanic lithosphere: Serpentinization is not isochemical. *Earth and Planetary Science Letters*, *430*, 75–85. https://doi.org/10.1016/j.epsl.2015.07.043

Mavromatis, V., Gautier, Q., Bosc, O., & Schott, J. (2013). Kinetics of Mg partition and Mg stable isotope fractionation during its incorporation in calcite. *Geochimica et Cosmochimica Acta*, *114*, 188–203. https://doi.org/10.1016/J.GCA.2013.03.024

Mavromatis, V., Purgstaller, B., Dietzel, M., Buhl, D., Immenhauser, A., & Schott, J. (2017). Impact of amorphous precursor phases on magnesium isotope signatures of Mg-calcite. *Earth and Planetary Science Letters*, *464*, 227–236. https://doi.org/10.1016/J.EPSL.2017.01.031

Mervine, E. M., Humphris, S. E., Sims, K. W. W., Kelemen, P. B., & Jenkins, W. J. (2014). Carbonation rates of peridotite in the Samail Ophiolite, Sultanate of Oman, constrained through ^{14}C dating and stable isotopes. *Geochimica et Cosmochimica Acta*, *126*, 371–397. https://doi.org/10.1016/j.gca.2013.11.007

Monnier, C., Girardeau, J., Le Mée, L., & Polvé, M. (2006). Along-ridge petrological segmentation of the mantle in the Oman ophiolite. *Geochemistry, Geophysics, Geosystems*, *7*, Q11008. https://doi.org/10.1029/2006GC001320

Monnin, C., Chavagnac, V., Ceuleneer, G., Boulart, C., & Hoareau, G. (2011). Characterization of hyperalkaline fluids produced by serpentinization of mantle peridotites in Oman and in Liguria (Northern Italy). *Mineralogical Magazine*, *75*, 1490.

Moody, J. B. (1976). Serpentinization: A review. *Lithos*, *9*, 125–138. https://doi.org/10.1016/0024-4937(76)90030-X

Nasir, S., Al Sayigh, A. R., Al Harthy, A., Al-Khirbash, S., Al-Jaaidi, O., Musllam, A., et al. (2007). Mineralogical and geochemical characterization of listwaenite from the Semail Ophiolite, Oman. *Chemie der Erde-Geochemistry*, *67*, 213–228. https://doi.org/10.1016/j.chemer.2005.01.003

Neal, C., & Stanger, G. (1983). Hydrogen generation from mantle source rocks in Oman. *Earth and Planetary Science Letters*, *66*, 315–320. https://doi.org/10.1016/0012-821X(83)90144-9

Neal, C., & Stanger, G. (1985). Past and present serpentinization of ultramafic rocks: An example from the Semail ophiolite nappe of northern Oman. In J. Drewer (Ed.), *The chemistry of weathering* (pp. 249–275). Dordrecht, Holland: D. Reidel Publishing Company.

Nicolas, A., Boudier, F., & France, L. (2009). Subsidence in magma chamber and the development of magmatic foliation in Oman ophiolite gabbros. *Earth and Planetary Science Letters*, *284*, 76–87. https://doi.org/10.1016/j.epsl.2009.04.012

Noël, J., Godard, M., Oliot, E., Martinez, I., Williams, M., Boudier, F., et al. (2018). Evidence of polygenetic carbon trapping in the Oman ophiolite: Petro-structural, geochemical, and carbon and oxygen isotope study of the Wadi Dima harzburgite-hosted carbonates (Wadi Tayin massif, Sultanate of Oman). *Lithos*, *323*, 218–237. https://doi.org/10.1016/J.LITHOS.2018.08.020

Oelkers, E. H., Berninger, U. N., Pérez-Fernàndez, A., Chmeleff, J., & Mavromatis, V. (2018). The temporal evolution of magnesium isotope fractionation during hydromagnesite dissolution, precipitation, and at equilibrium. *Geochimica et Cosmochimica Acta*, *226*, 36–49. https://doi.org/10.1016/j.gca.2017.11.004

Oskierski, H. C., Beinlich, A., Mavromatis, V., Altarawneh, M., & Dlugogorski, B. Z. (2019). Mg isotope fractionation during continental weathering and low temperature carbonation of ultramafic rocks. *Geochimica et Cosmochimica Acta*, *262*, 60–77. https://doi.org/10.1016/J.GCA.2019.07.019

Paukert Vankeuren, A. N., Matter, J. M., Stute, M., & Kelemen, P. B. (2019). Multitracer determination of apparent groundwater ages in peridotite aquifers within the Samail ophiolite, Sultanate of Oman. *Earth and Planetary Science Letters*, *516*, 37–48. https://doi.org/10.1016/J.EPSL.2019.03.007

Paukert, A. N., Matter, J. M., Kelemen, P. B., Shock, E. L., & Havig, J. R. (2012). Reaction path modeling of enhanced in situ CO_2 mineralization for carbon sequestration in the peridotite of the Samail Ophiolite, Sultanate of Oman. *Chemical Geology*, *330–331*, 86–100. https://doi.org/10.1016/j.chemgeo.2012.08.013

Pearce, C. R., Saldi, G. D., Schott, J., & Oelkers, E. H. (2012). Isotopic fractionation during congruent dissolution, precipitation and at equilibrium: Evidence from Mg isotopes. *Geochimica et Cosmochimica Acta*, *92*, 170–183. https://doi.org/10.1016/j.gca.2012.05.045

Pinilla, C., Blanchard, M., Balan, E., Natarajan, S. K., Vuilleumier, R., & Mauri, F. (2015). Equilibrium magnesium isotope fractionation between aqueous Mg^{2+} and carbonate minerals: Insights from path integral molecular dynamics. *Geochimica et Cosmochimica Acta*, *163*, 126–139. https://doi.org/10.1016/j.gca.2015.04.008

Power, I. M., Kenward, P. A., Dipple, G. M., & Raudsepp, M. (2017). Room temperature magnesite precipitation. *Crystal Growth & Design*, *17*, 5652–5659. https://doi.org/10.1021/acs.cgd.7b00311

Ryu, J.-S., Vigier, N., Decarreau, A., Lee, S.-W., Lee, K.-S., Song, H., & Petit, S. (2016). Experimental investigation of Mg isotope fractionation during mineral dissolution and clay formation. *Chemical Geology*, *445*, 135–145. https://doi.org/10.1016/j.chemgeo.2016.02.006

Saldi, G. D., Schott, J., Pokrovsky, O. S., Gautier, Q., & Oelkers, E. H. (2012). An experimental study of magnesite precipitation rates at neutral to alkaline conditions and 100–200 °C as a function of pH, aqueous solution composition and chemical affinity. *Geochimica et Cosmochimica Acta*, *83*, 93–109. https://doi.org/10.1016/J.GCA.2011.12.005

Santiago Ramos, D. P., Coogan, L. A., Murphy, J. G., & Higgins, J. A. (2020). Low-temperature oceanic crust alteration and the isotopic budgets of potassium and magnesium in seawater. *Earth and Planetary Science Letters*, *541*, 116290. https://doi.org/10.1016/j.epsl.2020.116290

Schauble, E. A. (2011). First-principles estimates of equilibrium magnesium isotope fractionation in silicate, oxide, carbonate and hexaaquamagnesium(2+) crystals. *Geochimica et Cosmochimica Acta*, *75*, 844–869. https://doi.org/10.1016/J.GCA.2010.09.044

Schott, J., Mavromatis, V., Fujii, T., Pearce, C. R., & Oelkers, E. H. (2016). The control of carbonate mineral Mg isotope composition by aqueous speciation: Theoretical and experimental modeling. *Chemical Geology*, *445*, 120–134. https://doi.org/10.1016/j.chemgeo.2016.03.011

Shirokova, L. S., Mavromatis, V., Bundeleva, I. A., Pokrovsky, O. S., Bénézeth, P., Gérard, E., et al. (2013). Using Mg isotopes to trace cyanobacterially mediated magnesium carbonate precipitation in Alkaline Lakes. *Aquatic Geochemistry*, *19*, 1–24. https://doi.org/10.1007/s10498-012-9174-3

Skarpelis, N. (2006). Lateritization processes of ultramafic rocks in Cretaceous times: The fossil weathering crusts of mainland Greece. *Journal of Geochemical Exploration*, *88*, 325–328. https://doi.org/10.1016/j.gexplo.2005.08.066

Snow, J. E., & Dick, H. J. B. (1995). Pervasive magnesium loss by marine weathering of peridotite. *Geochimica et Cosmochimica Acta*, *59*, 4219–4235. https://doi.org/10.1016/0016-7037(95)00239-V

Stanger, G. (1985). Silicified serpentinite in the Semail nappe of Oman. *Lithos*, *18*, 13–22. https://doi.org/10.1016/0024-4937(85)90003-9

Streit, E., Kelemen, P. B., & Eiler, J. (2012). Coexisting serpentine and quartz from carbonate-bearing serpentinized peridotite in the Samail Ophiolite, Oman. *Contributions to Mineralogy and Petrology*, *164*, 821–837. https://doi.org/10.1007/s00410-012-0775-z

Su, B.-X., Teng, F.-Z., Hu, Y., Shi, R.-D., Zhou, M.-F., Zhu, B., et al. (2015). Iron and magnesium isotope fractionation in oceanic lithosphere and sub-arc mantle: Perspectives from ophiolites. *Earth and Planetary Science Letters*, *430*, 523–532. https://doi.org/10.1016/j.epsl.2015.08.020

Teng, F.-Z. (2017). Magnesium isotope geochemistry. *Reviews in Mineralogy and Geochemistry*, *82*, 219–287. https://doi.org/10.2138/rmg.2017.82.7

Teng, F.-Z., Li, W.-Y., Ke, S., Marty, B., Dauphas, N., Huang, S., et al. (2010). Magnesium isotopic composition of the Earth and chondrites. *Geochimica et Cosmochimica Acta*, *74*, 4150–4166. https://doi.org/10.1016/j.gca.2010.04.019

Teng, F. Z., Li, W. Y., Ke, S., Yang, W., Liu, S. A., Sedaghatpour, F., et al. (2015). Magnesium isotopic compositions of international geological reference materials. *Geostandards and Geoanalytical Research*, *39*, 329–339. https://doi.org/10.1111/j.1751-908X.2014.00326.x

Tipper, E. T. T., Galy, A., Gaillardet, J., Bickle, M. J. J., Elderfield, H., & Carder, E. A. A. (2006). The magnesium isotope budget of the modern ocean: Constraints from riverine magnesium isotope ratios. *Earth and Planetary Science Letters*, *250*, 241–253. https://doi.org/10.1016/j.epsl.2006.07.037

Wang, W., Zhou, C., Liu, Y., Wu, Z., & Huang, F. (2019). Equilibrium Mg isotope fractionation among aqueous Mg^{2+}, carbonates, brucite and lizardite: Insights from first-principles molecular dynamics simulations. *Geochimica et Cosmochimica Acta*, *250*, 117–129. https://doi.org/10.1016/J.GCA.2019.01.042

Weyhenmeyer, C. E., Burns, S. J., Waber, H. N., & Matter, A. (2002). Isotope study of moisture sources, recharge areas, and groundwater flow paths within the eastern Batinah coastal plain, Sultanate of Oman. *Water Resources Research*, *38*(10), 1184. https://doi.org/10.1029/2000WR000149

Wimpenny, J., Colla, C. A., Yin, Q.-Z. Z., Rustad, J. R., & Casey, W. H. (2014). Investigating the behaviour of Mg isotopes during the formation of clay minerals. *Geochimica et Cosmochimica Acta*, *128*, 178–194. https://doi.org/10.1016/j.gca.2013.12.012

Wimpenny, J., Gíslason, S. R., James, R. H., Gannoun, A., Pogge Von Strandmann, P. A. E., & Burton, K. W. (2010). The behaviour of Li and Mg isotopes during primary phase dissolution and secondary mineral formation in basalt. *Geochimica et Cosmochimica Acta*, *74*, 5259–5279. https://doi.org/10.1016/j.gca.2010.06.028

Young, E. D., & Galy, A. (2004). The isotope geochemistry and cosmochemistry of magnesium. *Reviews in Mineralogy and Geochemistry*, *55*, 197–230.